

## Control of Bacterial Attachment by Fracture Topography

Amar Velic<sup>a</sup>, Asha Mathew<sup>a</sup>, Peter Hines<sup>b</sup>, Prasad K.D.V Yarlagadda<sup>a1</sup>

<sup>a</sup> School of Chemistry, Physics and Mechanical Engineering, Science and Engineering Faculty, Queensland University of Technology, Brisbane, Australia

<sup>b</sup> Central Analytical Research Facility, Institute for Future Environments, Queensland University of Technology, Brisbane, Australia

y.prasad@qut.edu.au,

### Abstract

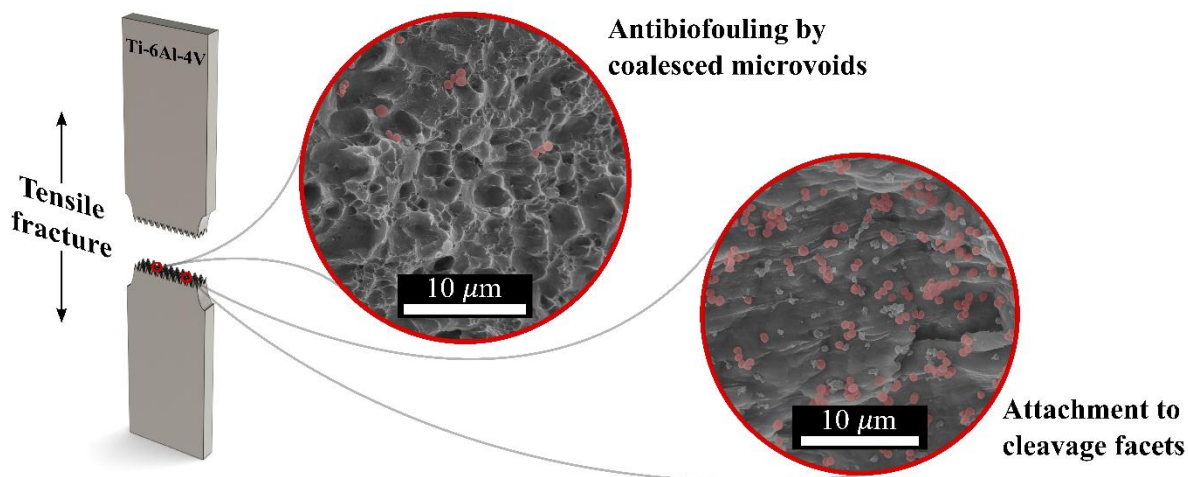
In the biomedical arena, bacterial fouling is a precursor to complications such as implant infection and nosocomial infection. These complications are further compounded by biochemical mechanisms of resistance that threaten the action of traditional antibacterial strategies. Accordingly, antibacterial property by physical, not biochemical, mechanisms of action are becoming increasingly popular and promising. The present work falls in line with this paradigm shift. Here, a Ti-6Al-4V microtextured surface is manufactured by destructive tension at three different cross-head speeds, probed with scanning electron microscopy and multifocus optical microscopy, and treated with *Staphylococcus aureus* to study bacterial attachment. The fractographic study of Ti-6Al-4V revealed the presence of dual-mode fracture characterised by regions of both ductile, microvoid coalescence and brittle, cleavage facets. Based on load-extension curves, quantitative roughness data, and qualitative SEM visualisation, it was evident that cross-head speed modulated fracture behaviour such that increased speed produced more brittle fracture whilst slower speeds produced more ductile fracture. The topography associated with ductile fracture was found to possess notable antibiofouling property due to geometric constraints imposed by the coalesced microvoids. Accordingly, fracture at low cross-head speeds (1mm/min and 10mm/min) yielded significant reduction in bacterial attachment, whilst fracture at high cross-head speeds (100mm/min) did not. The greatest reduction (~72%) was achieved at a cross-head speed of 1mm/min. These findings suggest that antibiofouling property can be elicited by fracture and further 'tuned' by fracture speed. Discovery of this novel, albeit simple, avenue for topography-mediated antibacterial property calls for further research into alternate techniques for the manufacture of 'physical antibacterial surfaces'.

Graphical abstract

fx1

---

<sup>1</sup> Ph: +61 7 3138 5167



### Keywords

titanium alloy; fractography; bacterial adhesion; staphylococcus aureus; antibiofouling; topography

## 1. INTRODUCTION

The attachment of bacteria to biomedical surfaces is a precursor to significant healthcare complications. Attachment is the foundational step toward the formation of a complex, multicellular community known as a 'biofilm'. This collective arrangement of bacteria confers resistance to all manner of physiological stresses making their eradication very difficult (Boyle, Heilmann, van Ditmarsch, & Xavier, 2013; Vega & Gore, 2014). The consequences of this are perhaps best appreciated in the context of medical device fouling, where biofilms lead to antibiotic-resistant infection that necessitates costly and complicated treatment (Ribeiro, Monteiro, & Ferraz, 2012). In addition, biofilm resistance also enables pathogens to persist for up to several weeks on the surfaces of hospital bedding, furnishings and equipment, even despite dry conditions and cleaning with biocides and disinfectants (Neely & Maley, 2000; Vickery et al., 2012; Weinstein & Hota, 2004). Here they put susceptible healthcare patients at risk of nosocomial infections by surface-to-patient cross-contamination, mostly via the hands and gloves of health care workers (Boyce, 2007; Weber, Rutala, Miller, Huslage, & Sickbert-Bennett, 2010; Weinstein & Hota, 2004).

These implications to device-related infection and nosocomial infection are the major motives underlying the pursuit of antibacterial surfaces for biomedical application. The design of such surfaces is experiencing a paradigm shift due to the increasing prevalence of biochemical mechanisms of resistance that invalidate 'traditional' antibacterial strategies that

also operate on biochemical mechanisms (Brown & Wright, 2016; Davies & Davies, 2010). Accordingly, there is a growing interest for mechanisms of action that are distinct from these conventional approaches. A significant research focus has been placed on so-called ‘physical antibacterial surfaces’ which rely on physical mechanisms of action elicited by modification to surface architecture or, more simply, ‘texturing’ (Hasan, Crawford, & Ivanova, 2013).

When texturing is performed at the microscale ( $\mu$ ) the resultant antibacterial property is ‘antibiofouling’. This describes an ability to deter the attachment and subsequent proliferation of bacteria and other microorganisms. The mechanism underlying microtexture antibiofouling is most popularly elucidated by the ‘attachment point theory’ (Scardino, Guenther, & de Nys, 2008). This theory posits that the cell’s physical interaction with the topography – in terms of the degree of attraction and strength of adsorption - relies upon interfacial area (Dunne, 2002). Hence, by modulating the cell-accessible surface area, interaction and attachment can be enhanced or suppressed without biochemical modification (Valle et al., 2015). For instance, when the dimensions of the microtexture are larger than the size of the fouling microorganism, microtexturing contributes additional surface area available for contact and increased interaction. Consequently, these microtextures have been observed to increase attachment numbers for bacteria (Hou, Gu, Smith, & Ren, 2011; Komaromy et al., 2012; Valle, et al., 2015; Whitehead, Colligon, & Verran, 2005) and other microorganisms (Callow et al., 2002; Carman et al., 2006; Hoipkemeier-Wilson et al., 2004), relative to a flat surface. Conversely, when the feature size and spacing are reduced to near- or sub-cell dimensions, the target microorganism can only establish relatively weak interaction on feature tops, whilst the interstitial area between features is physically blocked-off to the body of the cell. For various bacteria (Friedlander et al., 2013; Valle, et al., 2015; Vasudevan, Kennedy, Merritt, Crocker, & Baney, 2014; Whitehead, et al., 2005; Xu & Siedlecki, 2012) and other microorganisms (Carman, et al., 2006; Petronis, Berntsson, Gold, & Gatenholm, 2000; Scardino, Harvey, & De Nys, 2006; Schumacher et al., 2007), these microtextures reduce attachment relative to a flat control. Based on extensive study and review, researchers have stipulated that microtexture dimensions approximately 50-90% of the target organism’s major dimension result in optimal antibiofouling (Scardino & de Nys, 2011). There are negative returns with further reduction (Katsikogianni, 2004).

To elicit this topography-mediated antibiofouling, microtexturing is most popularly carried out by lithography techniques, typically UV lithography followed by soft lithography (Bixler, Theiss, Bhushan, & Lee, 2014; Carman, et al., 2006; Chung et al., 2007; Vasudevan, et al., 2014; Xu & Siedlecki, 2012). Microtexturing by ablation of polymer and metallic substrates with gas or solid-state laser is also reasonably common (Fadeeva et al., 2011; Truong et al., 2012; Valle, et al., 2015). That being said, despite their widespread use, the aforementioned manufacturing techniques have some drawbacks. In the case of lithography, geometric complexity can be difficult to achieve and production can involve many time-intensive fabrication steps (Zhang et al., 2014). On the other hand, laser ablation requires highly customised, expensive equipment and alters surface chemistry through oxidation (Fiorucci, López, & Ramil, 2015). Both techniques are also more commonly associated with polymers, which offer limited scope of application in the biomedical arena. These existing approaches are thus either cumbersome, or simply invalid, for studying the isolated effects of topography on bacterial adhesion to metallic surfaces.

Fabrication of a metallic textured surface may be carried out more simplistically with tensile fracture. Tensile fracture involves a few, simple steps that can be executed swiftly, without reliance on expensive, state-of-the-art clean room facilities. Broadly speaking, a fracture texture will take on a topography that stems from either ductile, brittle or dual-mode fracture. In ductile fracture, the topography appears rough and dimpled due to the nucleation, growth and coalescence of microvoids during plastic flow (Parrington, 2002). In brittle fracture, flat and featureless ‘cleavage’ facets appear in the topography due to transgranular fracture along well-defined crystallographic planes (Mudry, 1987). Compared to ductile fracture, brittle fracture is characterised by rapid crack propagation with very little plastic deformation and minimal adsorption of energy (Campbell, 2012). In the dual-mode fracture, both textural features are apparent. More specifically, ‘quasi-cleavage’ facets, which are not necessarily restricted to well-defined planes, tend to be separated by voids or regions of microvoid coalescence (Kumar, Roberts, & Wilkinson, 2007). Of course, the nature of the fracture mode - and thus its resultant topography - depends on various factors related to the properties of the material and the conditions of the loading. For instance, metals with HCP and BCC crystal structures are more prone to brittle fracture than FCC counterparts (Mudry, 1987). Also, at lower temperatures, the fracture mode transitions from ductile to brittle (Gerberich & Yang, 2003). Likewise, lower deformation rates induce more ductile fracture whilst brittle fracture is more likely to occur at extremely high loading rates (Gerberich &

Yang, 2003; Pokluda & Šandera, 2010). By enabling loose control over the failure mode, these material properties and loading conditions may offer avenues to ‘tune’ the topography of a fracture texture to achieve antibiofouling property.

This notion creates the basis for the experimental framework presented in this study. Accordingly, a microscale topography is manufactured by tensile fracture of Ti-6Al-4V coupons at variable loading rates. By adjusting the cross-head speed, from quasi-static to dynamic, we modulate the fracture mode to achieve different topographies. The antibiofouling efficacy, against *S. aureus*, is evaluated for each topography by comparison to flat controls. It is shown that lower cross-head speeds can be used to fabricate textured surfaces with an inherent, topography-mediated antibiofouling property which significantly reduces the attachment of bacteria.

## 2. MATERIALS AND METHODS

### 2.1. Materials and manufacturing

Annealed titanium alloy Ti-6Al-4V (grade 5) was chosen as the model material for its attractive properties and broad biomedical utility, evidenced by widespread use in joint replacement, fracture fixation, dental implants and surgical tools (Elias, Lima, Valiev, & Meyers, 2008; Rack & Qazi, 2006). Description of the mechanical properties and alloy composition of Ti-6Al-4V can be found in ASTM B265-15 (ASTM International, 2015). Notably, Ti-6Al-4V comprises  $\alpha$  and  $\beta$  phases, which are stabilised at room temperature by the inclusion of aluminium (5.5 – 6.5 w.t. %) and vanadium (3.5 – 4.5 w.t. %), respectively (Murr et al., 2009).

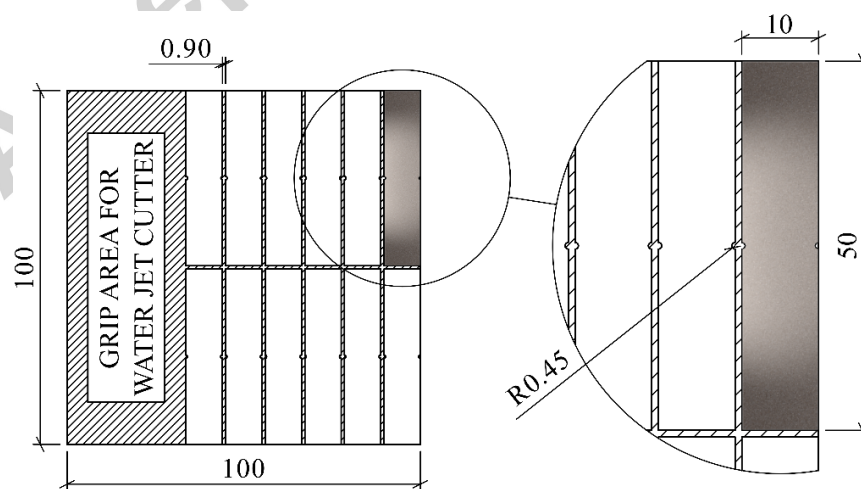
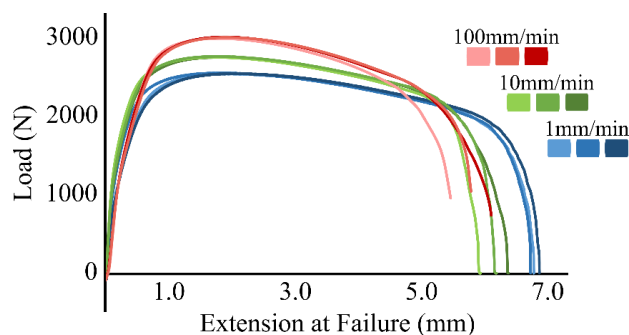


Figure 1: Specification drawing for manufacture of coupon specimens (greyscale figure) (1.5 column)

Raw material was originally sourced in the form of 100×100×0.8mm sheets. From the master sheets, coupons and flat controls were machined by a water jet cutter with a stream diameter of 0.9 mm. Flat controls were designed as 5×10×0.8mm rectangular disks. For the design of the coupons, a standard sheet-type specimen was approximated as per ASTM E8/E8M-16a (ASTM International, 2016). The standard was adhered to only where necessary to ensure consistency, permitting some design simplifications be made to facilitate fabrication. Accordingly, a coupon size of 50×10×0.8mm was defined to maximise yield-per-sheet whilst simultaneously providing sufficient clamping area for wedge grips (Figure 1). The cross-sectional area in the centre of the coupon was reduced by two semicircular stress-raisers in order to constrain the fracture. These notches were inspected for burrs or excessive roughness to minimise irregularities that threatened the validity and consistency of the results (ASTM International, 2016). Prior to testing, the reduced cross sectional area was measured to ensure that the width and thickness were within good accuracy (i.e.  $\pm 0.1$ mm).

The testing procedure generally followed prescribed methods (ASTM International, 2016). Briefly, the INSTRON 5569A load frame was exercised to non-transient conditions and force was zeroed to correspond with no gripping. A specimen was then loaded into the wedge grips, such that the upper and lower grips were displaced 5mm above and below the reduced central section, respectively. The wedge grips were aligned centrally with the specimen to ensure purely axial tension. Once positioned accurately, the grips were tightened with a pre-compression of 85N. A predefined, standard tensile testing method in Bluehill<sup>®</sup>2 was executed at cross-head speeds of 1mm/min, 10mm/min and 100mm/min until complete fracture. These speeds covered strain rates from quasi-static to highly dynamic. Three coupons were fractured at each speed. The extension-load curves were inspected prior to further study, to confirm the consistency and repeatability of fracture results (Figure 2).



**Figure 2: Load-extension curves for tensioning at crosshead speeds of 1, 10 and 100mm/min (colour figure) (single column)**

## 2.2. Surface characterisation

Two techniques were applied to characterise the fracture surfaces, namely, scanning electron microscopy (SEM) and multifocus optical microscopy. High-resolution electron micrographs were captured using a field-emission SEM (JEOL JSM-7001F) with operating parameters set in the vicinity of 20kV accelerating voltage and ‘medium’ (11) spot size. The hierarchical nature of the surface was surveyed with magnifications ranging from 1000× to 15,000×. This was carried out at across various representative locations, along the longitudinal centreline of the fracture surface.

Lower magnification images with extended depth of field were obtained using a motorized stereo microscope (Leica M125) with Leica Application Suite (LAS) integration. Z-Stack parameters (start-end positions, no. of steps) were adjusted on the LAS MultiFocus module to automatically capture and compile 250 image steps from the lowermost, to the uppermost, focal points on the fracture topographies. This produced a single, crisp, composite image with greatly extended focus – a so-called ‘montage’. A zoom settings of 5× was used on a 1.0× plan-apochromatic objective lens. With Digital Surf Mountains<sup>®</sup>Map software, the montages were converted into three-dimensional surface maps and post-processed to calculate ISO 25178 surface texture parameters for quantitative comparison.

## 2.3. Bacterial growth and incubation

*Staphylococcus aureus* (ATCC 25923) was used as the model microorganism in this study given its prevalent fouling on hospital surfaces and implant devices (Vickery, et al., 2012). For instance, *S. aureus* is the leading cause of hospital-acquired surgical site infections, and second leading cause of nosocomial bacteraemia and pneumonia (Klein, Smith, & Laxminarayan, 2007). It is also the most common etiological agent in prosthetic joint infections, as well as infections associated with internal and external fixators (Lora-Tamayo et al., 2013; Montanaro et al., 2011).

Prior to each bacterial attachment experiment, cultures were refreshed on nutrient agar from stocks (Oxoid, Australia). Fresh bacterial suspensions were grown overnight, in 5 ml of nutrient broth, at 37°C (Oxoid, Australia). Bacterial cells were collected at the logarithmic stage of growth and the suspensions were adjusted to OD<sub>600</sub>= 0.3. Before incubation on sterilised fractured coupons, the bacteria suspension in PBS was adjusted to OD<sub>600</sub>=1.

Flat controls and coupons fractured at different cross-head speeds (1mm/min, 10mm/min and 100mm/min, n=3) were totally submerged in diluted *S. aureus* test solution (1:10) and incubated at 37°C for a minimum of 18h. The cell suspension was then removed and fractured coupons were fixed with 3% glutaraldehyde for 3 hours, rinsed three times with 0.1M cacodylate buffer, followed by dehydration in a graded series of ethanol (20%, 40%, 60%, 80%, 90% and 100%) and drying with hexamethyldisilazane. After drying, samples were gold-coated, mounted and observed under SEM to study antibiofouling behaviour.

#### 2.4. Bacterial attachment studies

Study of bacterial attachment followed standard methods found in Hoipkemeier-Wilson, et al. (2004) and Callow, et al. (2002). Accordingly, attached *S. aureus* cells were visualised with SEM (JEOL JSM-7001F) and quantified by manual interval counting. In terms of operating parameters, SEM was used with a 20kV accelerating voltage, a 'medium' (11) spot size and a 5mm working distance. To ensure a good representation of each sample, attachment was surveyed along the longitudinal centreline with 20 fields of view evenly spanning the entire length of the fracture surface (Figure 3). For all fracture speeds, this length measured approximately 4mm, hence an even interval of 0.2mm was chosen. Any fields marred by dust particles were neglected, and the region next to the disruption was imaged. A magnification of 3,000× was chosen to capture a reasonable quantity of bacteria (i.e.  $<10^3$ ). For consistency and comparison, the same interval (0.2mm) and magnification (3,000×) were used to study *S. aureus* attachment along the centreline of flat control surfaces. Using three samples for each case (1mm/min, 10mm/min, 100mm/min and control) and 20 fields of view per sample, a total of 240 fields were examined. The number of attached bacteria per field was quantified and normalised to projected surface area using the planar dimensions of the field (Figure 3). Area-normalised attachment (*bacteria/mm<sup>2</sup>*) was compared across all cases to ascertain any significant reduction in attachment that would indicate an antibiofouling property.

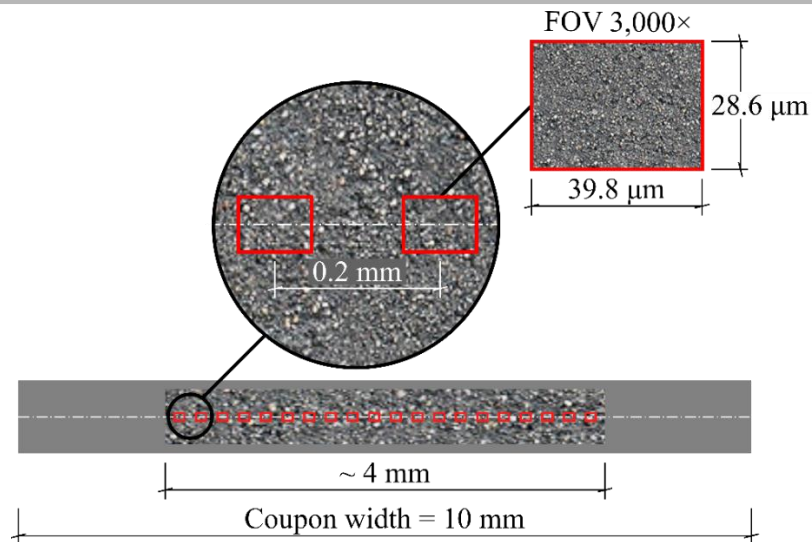


**Figure 3: Study of bacterial attachment on fracture surfaces by manual count with SEM (colour figure) (1.5 column)**

## 2.5. Statistical analysis

Results are expressed as mean $\pm$ standard deviation. Statistical significance was assessed using one-way ANOVA followed by post-hoc assessment using the Tukey HSD method.  $p$  values of  $<0.05$  were considered statistically significant. In all studies, the minimum sample size was three. For bacterial attachment studies, 20 fields of views were examined per sample, amounting to 60 field of view per cross-head speed.

### 3. RESULTS AND DISCUSSION

#### 3.1. Fractography and characterisation

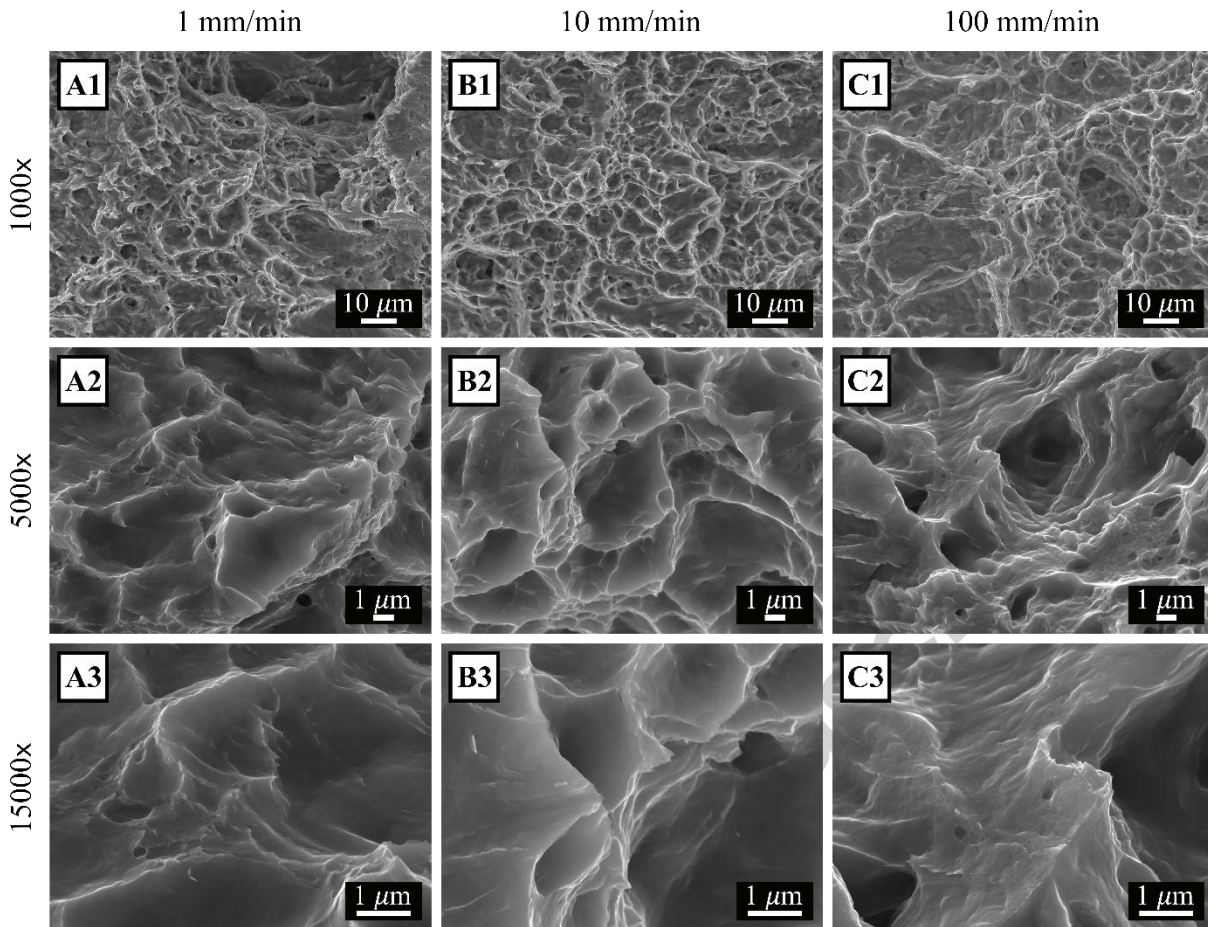


**Figure 4: Successive magnification SEM micrographs of fracture surface at different cross-head speeds (A) 1 mm/min (B) 10 mm/min (C) 100 mm/min (greyscale figure) (2 column)**

Scanning electron micrographs of the typical fractures produced at different cross-head speeds are shown in Figure 4. These illustrate topography at magnifications between 1000x and 15000x. The successive magnification emphasises the hierarchical quality of the surface. Several previous studies have linked hierarchical topographies - natural and synthetic - to antibiofouling property by their enhanced ability to support homogenous wetting (Barthlott & Neinhuis, 1997; Fadeeva, et al., 2011; Lafuma & Quere, 2003). Moreover, the surface morphology here demonstrated signs of a dual-mode fracture.

This was to be expected of annealed Ti-6Al-4V. This alloy typically comprises mainly equiaxed grains of  $\alpha$ -phase, with some  $\beta$ -phase settled along grain boundaries (Patil et al., 2016). Together, these phases facilitate a dual-mode fracture. It is suggested that microvoids nucleate at the  $\alpha/\beta$  interface, and subsequently grow and coalesce in a ductile fashion (Yang,

Wang, Lin, Zhao, & Ma, 2015). Conversely, ‘cleavage-like’ features are believed to be formed primarily by transgranular fracture of  $\alpha$  grains (Everaerts, Verlinden, & Wevers, 2016; Ivanova, Biederman, & Sisson, 2002). This is underpinned by their HCP crystal structure which can facilitate cleavage on the basal (0002) crystallographic plane (Mudry, 1987). Accordingly, the fracture texture of Ti-6Al-4V demonstrates coalesced microvoids separated by quasi-cleavage facets, as seen in Figure 5. This is in agreement with previous reports of titanium fracture (Attar, Calin, Zhang, Scudino, & Eckert, 2014; Piveta, Montandon, Ricci, & Nagle, 2012).

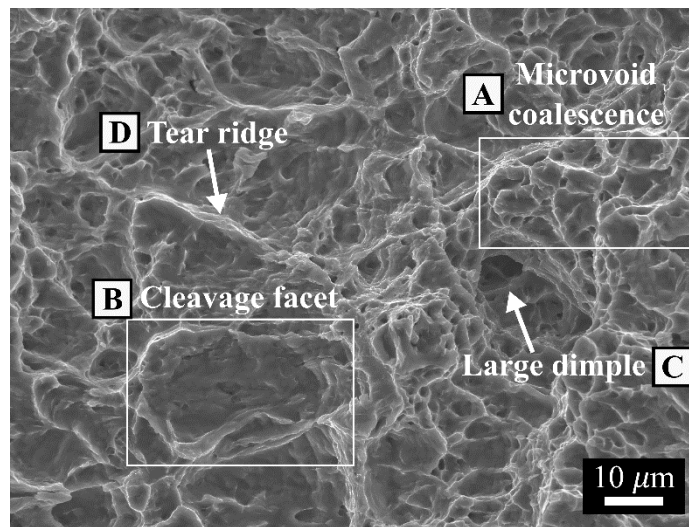


**Figure 5: Fractographic study via scanning electron microscopy (A) Microvoid coalescence (B) Quasi-cleavage facet (C) Large, equiaxed dimple (D) Tear ridge. Exemplar is specimen fractured at 100 mm/min (greyscale figure) (single or 1.5 column)**

These fracture modes depend on the applied cross-head speed and resultant strain rate. Here, the loading conditions range from quasi-static to dynamic. This is accompanied by several changes related to the deformation mechanisms, mechanical properties and fracture mode of Ti-6Al-4V. Fundamentally, the dominant deformation mechanism changes from dislocation motion to the formation of localised shear bands (Lee, Lin, & Huang, 2006). These shear bands are formed in adiabatic heating, that also results in thermal softening and reduced work hardening. Other mechanical implications of increasing strain rate to Ti-6Al-4V include increased yield stress and flow stress. This is true in quasi-static and dynamic conditions (Follansbee & Gray, 1989; Lee, et al., 2006). Present results seem to agree with these phenomena. Indeed, increasing the cross-head speed resulted in increased yield and ultimate force values (Figure 6). Increased strain rate has also been previously reported to modulate topography. Lee, et al. (2006) reported a primarily ductile fracture of Ti-6Al-4V,

with dimples that decreased in depth, radius and spacing as strain rate increased in dynamic conditions. In agreement, an  $\alpha/\beta$  titanium alloy reported by Yang, et al. (2015) showed more dense microvoids, that were smaller in radius and depth with increasing quasi-static strain rate due to overall greater strain and deformation of the voids at lower strain rates. Lastly, Lee, Chen, Lin, and Lu (2010) demonstrated the emergence of faceted features indicative of brittle fracture due to changes in dynamic strain rate. These studies suggest that strain rate has implications for the formation of faceted features, and also for the dimensions of coalesced microvoids.

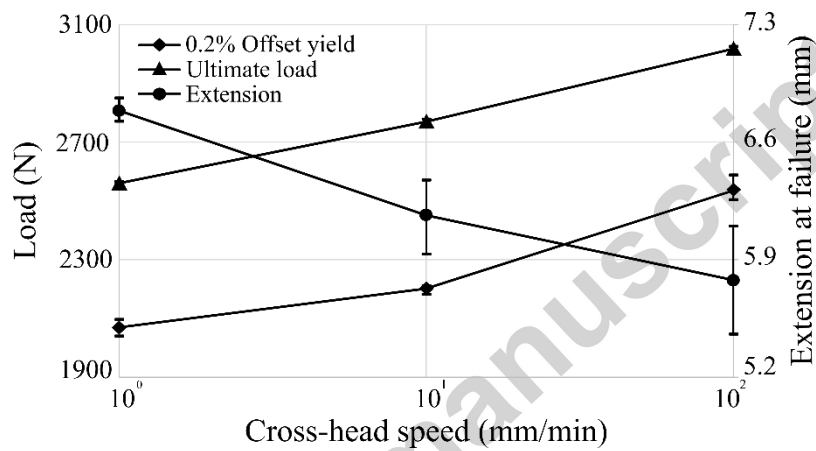


**Figure 6: Effect of cross-head speed on the mechanical properties of Ti-6Al-4V in terms of ultimate load, yield load and maximum extension (shown on logarithmic scale) (greyscale figure) (single or 1.5 column)**

To provide some quantitative elucidation of the proportion of quasi-cleavage facets and/or size of microvoids with respect to cross-head speed, multifocus optical microscopy was employed.

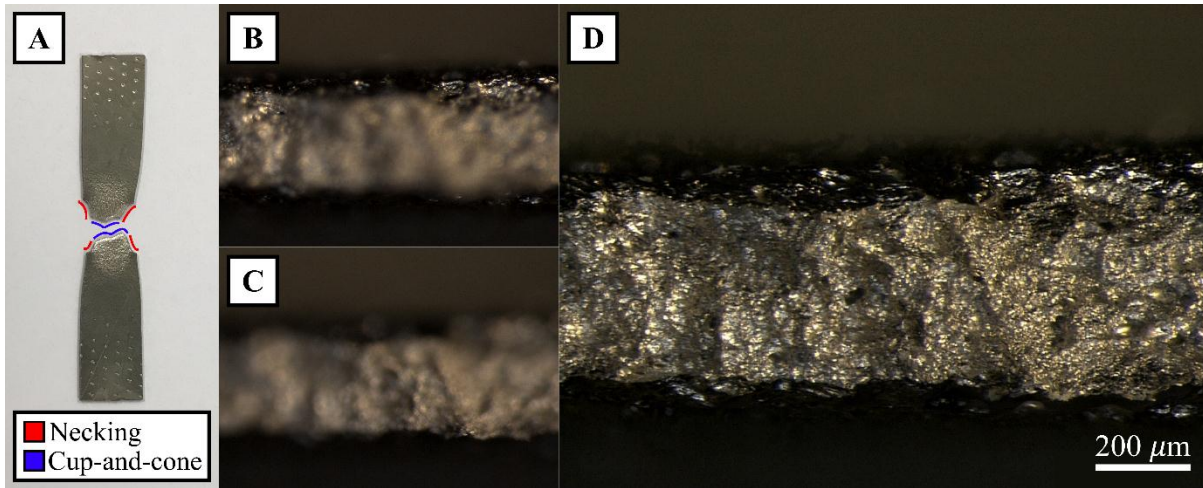


**Figure 7: Fractographic study via multifocus optical microscopy (A) Fractured tensile coupon emphasising cup-and-cone symmetry and necking regions (B) Photomicrograph at lower focal plane of Z-stack (C) Photomicrograph at upper focal plane of Z-stack (D) Composite, montage photomicrograph. Exemplar is specimen fractured at 100 mm/min (colour figure) (2 column)**

Studying the fracture pattern at macroscopic scales, the ductile fracture mode was most prominent, as evidenced by the shear lip and so-called ‘cup-and-cone’ fracture indicative of significant plastic deformation (Figure 7a). Due to this plastic deformation, the resulting free surface possessed significant height variability, which was best captured through focus stacking (Figure 7b-d). At this low-power magnification, signs of ductile fracture are visually dominant. The surface is marked with a rough, dimpled appearance characteristic of microvoid coalescence. Surface roughness calculated from these images is plotted in Figure 8. As seen, both the height range ( $S_p + S_v$ ) and mean height ( $S_a$ ) are reduced with increased cross-head speed. Hence, these results seem to support the notion that higher loading rates elicit a less rough surface characteristic of a more brittle fracture (Gerberich & Yang, 2003). Based on earlier discussion, this results can be explained by two effects related to the dual-mode fracture of Ti-6Al-4V. Firstly, there is more formation of flat and featureless facets due to exacerbation of cleavage fracture at high deformation rates (Pokluda & Šandera, 2010). Secondly, there is reduced growth and coalescence of voids due to rapid propagation and lower deformation, thus forming smaller, shallower and denser microvoids (Yang, et al., 2015). These two effects are likely resulting in a lower surface roughness in the case of faster cross-head speeds, as shown in Figure 8. Conversely, lower speed fracture produces a surface with higher roughness. This reflects a more ductile fracture with coalesced microvoids that are larger, deeper and less densely packed due to the increased deformation before and during fracture (Yang, et al., 2015). Trends from Figure 6 seem to align with this elucidation, showing that higher loading rates result in reduced extension indicative of more brittle failure

with lower energy adsorption. This elucidation was further evaluated by comprehensive SEM imaging applied to study bacterial attachment.

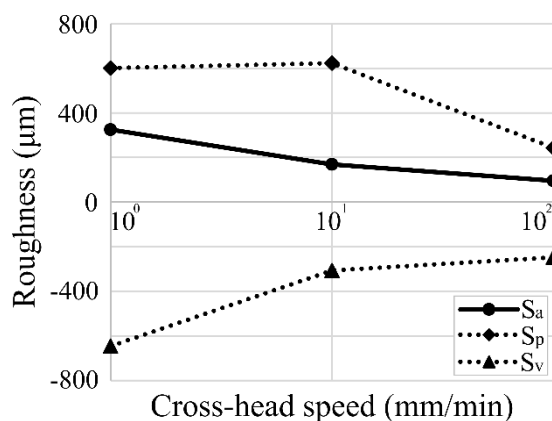


**Figure 8: Mean height ( $S_a$ ), maximum-peak ( $S_p$ ) and maximum-valley ( $S_v$ ) roughness of fracture surfaces (greyscale figure) (single column)**

### 3.2. Bacterial attachment studies

Interval counting demonstrated a reduction in *S. aureus* attachment on textured fracture surfaces relative to non-textured, flat controls (Figure 9). The reduction was dependent on the cross-head speed at which the fracture surface was produced. The 1mm/min, 10mm/min and 100mm/min fracture surfaces reduced average area-normalised attachment by 72%, 43% and 5%, respectively. These reductions were only statistically significant in the case of 1mm/min and 10mm/min cross-head speeds. Nonetheless, these results imply that fracture surfaces possess an antibiofouling property that can be modulated by cross-head speed. Given there is no chemical modification, the antibiofouling property can be attributed to a physical mechanism of action related to topography.

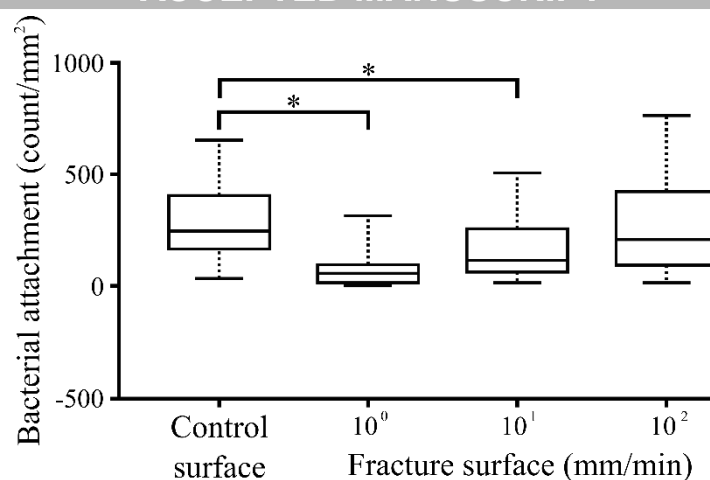


**Figure 9: Area-normalised counts of bacteria attached on control and fracture surfaces. \* indicates a statistically significant ( $p$ -value  $<0.05$ ) antibiofouling effect relative to the control surface, (greyscale figure) (single or 1.5 column)**

This mechanism appears to be more active in one of the two topographies that stem from dual-mode fracture. Signs of both ductile and brittle fracture can be found at all cross-head speeds, as seen in Figure 10. Comparing regions that are microvoid-dominant with those that are cleavage-dominant reveals a general trend that *S. aureus* settles less on the former than the latter. This can be explained in the context of the attachment point theory (Scardino, et al., 2008). Microvoid coalescence yields a surface that is highly textured and has characteristic dimensions that are near- or sub-bacterial in size. The *S. aureus* cells thus interact through reduced interfacial area, minimising the probability of attachment relative to a flat control (Xu & Siedlecki, 2012). Cleavage facets, on the other hand, produce a relatively featureless surface. These regions more closely resemble a flat surface and hence exhibit little or no relative antibiofouling property. It thus follows that the overall degree of antibiofouling is determined significantly by the proportion of these different topographies.

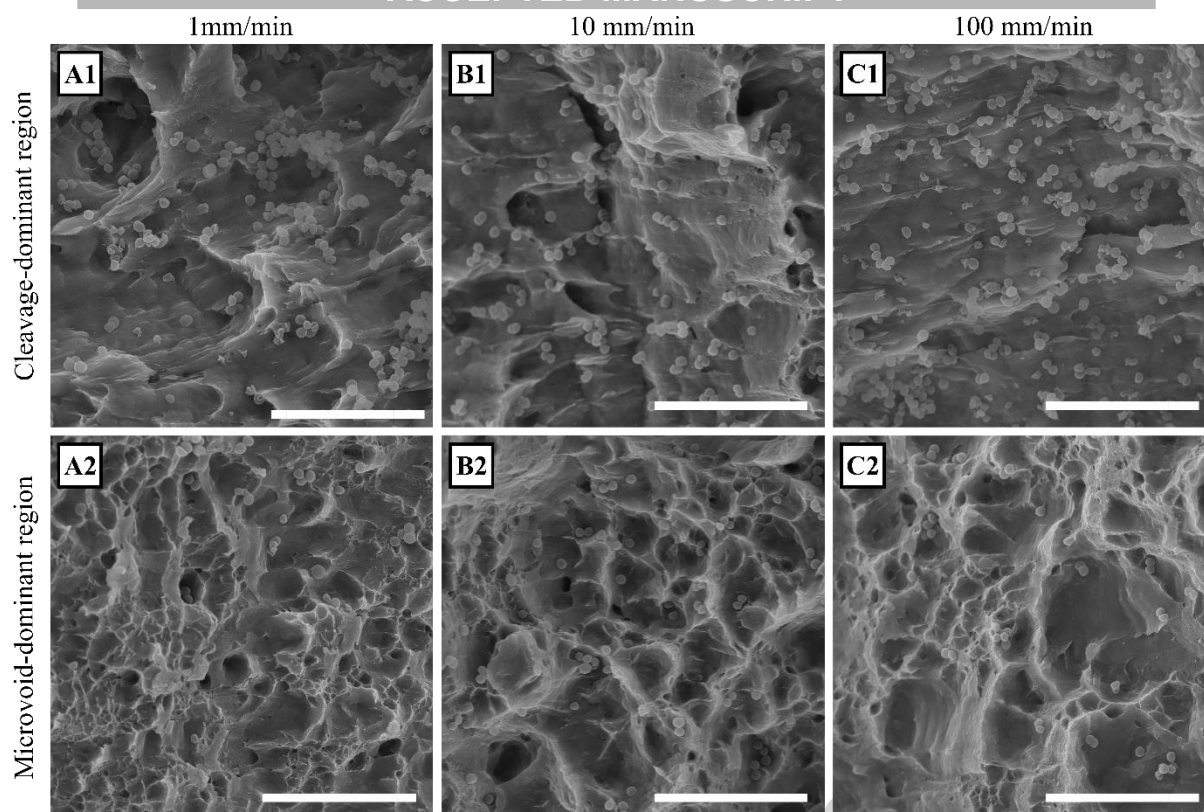


**Figure 10: Bacterial attachment on flat cleavage facets (A-C1) and antibiofouling on coalesced microvoids (A-C2). All scale bars are  $10\mu\text{m}$ . (greyscale figure) (2 column)**

As alluded earlier, lower cross-head speeds have a higher proportion of microvoid coalescence, whilst higher cross-head speeds have a higher proportion of quasi-cleavage. It is likely that this proportionality underlies the differential antibiofouling in the study. This notion is further reflected in the micrographs of Figure 11 which reveal that increasing cross-head speed elicits more brittle fracture. The effect is best seen in Figure 11c which shows fields of view representative of the overall fracture produced at 100mm/min. At this cross-head speed, the topography is relatively flat and featureless, due to the increase of the proportion of cleavage fracture. Though the texture still shows some signs of a dual-mode fracture, brittle failure mechanisms play a dominant role, exacerbated by the high deformation rate (Pokluda & Šandera, 2010). These observations are in good agreement with earlier roughness results (Figure 8) which indicated an overall lower mean roughness ( $S_a$ ) at increasing cross-head speeds. With more cleavage formation, the high cross-head speed of 100mm/min accommodates bacterial attachment numbers similar to the unmodified control surface (Figure 9).

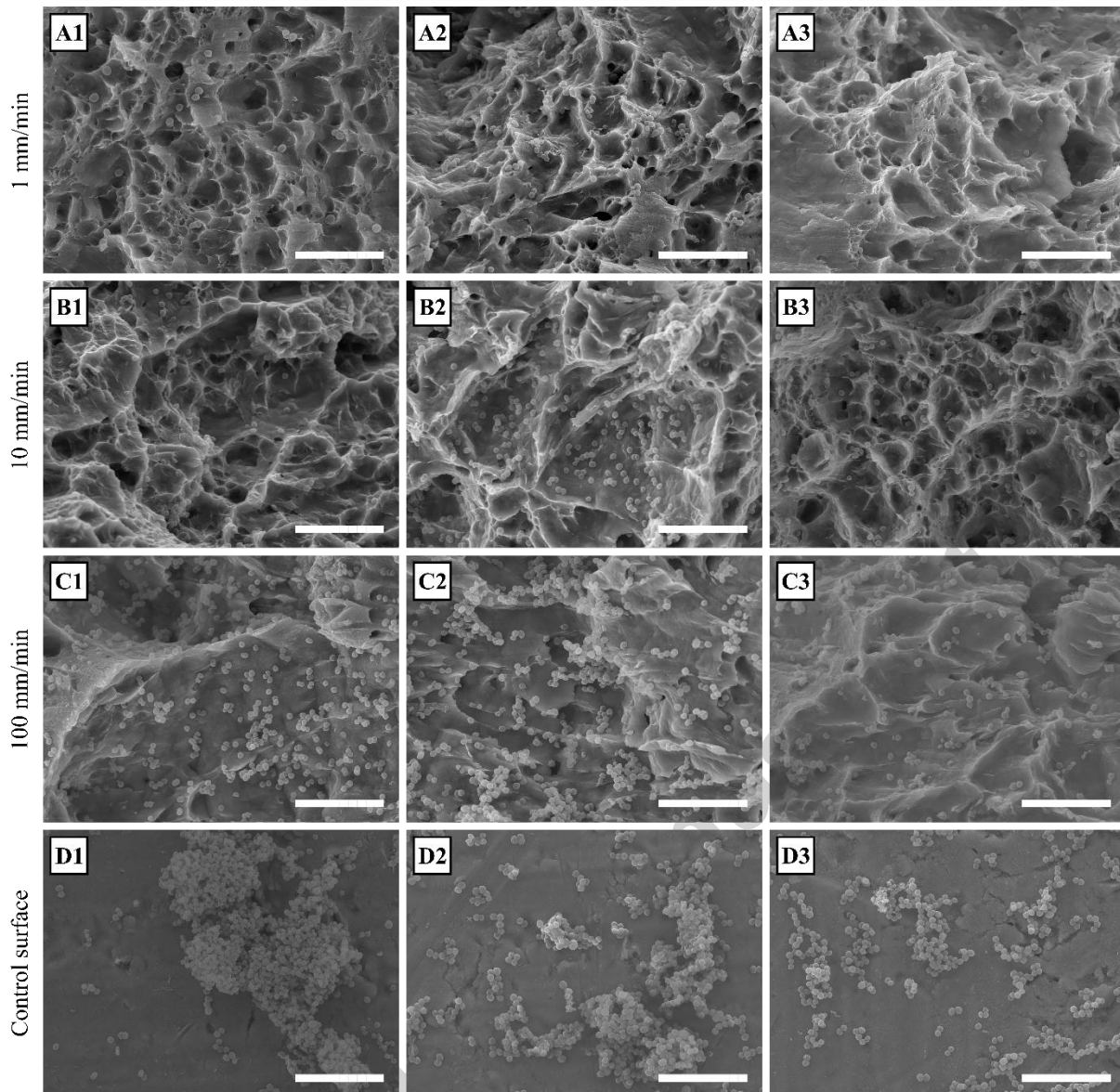


**Figure 11: SEM micrographs of bacterial attachment on fracture and control surfaces (A) 1 mm/min (B) 10 mm/min (C) 100 mm/min (D) Flat control. All scale bars 10 $\mu$ m, (greyscale figure) (2 column)**

Conversely, fractures at 1mm/min and 10mm/min show a greater proportion of ductile fracture. This is evidenced in Figure 11a-b where the surface appears markedly textured. With overall more microvoid coalescence, these textures are able to inhibit *S. aureus* attachment relative to the unmodified controls. The enhanced antibiofouling property at the cross-head speed of 1mm/min is likely due to the specific size of the microvoids generated. Recall, microvoids become smaller and more closely spaced at faster loading rates due to less plastic deformation before and during fracture (Yang, et al., 2015). Furthermore, texture dimensions at 50-90% of the target cell diameter are ideal for antibiofouling against a range of microorganisms (Scardino & de Nys, 2011). Though difficult to infer visually from the ‘busy’ SEM micrographs, it is suggested that the 1mm/min condition creates texture with

characteristic dimensions that are closest within this optimal range. This is supported by roughness data in Figure 8 which shows that mean height ( $S_a$ ) at 1mm/min is most proximate to the diameter of the *S. aureus* cells (i.e.  $\sim 0.5\text{-}1\mu\text{m}$ ). Whilst subtle, this variation in the texture geometry could indeed explain the significant bacterial antibiofouling difference between fractures at 1mm/min and 10mm/min which are both microvoid dominant (Hou, et al., 2011; Komaromy, et al., 2012; Valle, et al., 2015; Whitehead, et al., 2005).

Evidently, the mechanism that underpins this antibiofouling is based on a simplistic geometric mismatch between the bacteria size versus texture size, as elucidated by the attachment point theory. Hence, this mechanism may not be robust to the diversity of ‘nuances’ involved in all types of cell-surface interaction. For example, Friedlander, et al. (2013) brought to light the profound structural function of flagella in bacterial attachment of *Escherichia coli*. Flagella are able to create a dense, fibrous ‘buffer’ over unfavourable topography, and can reach into small interstitial crevices otherwise inaccessible to the body of the bacteria. As such, they enable the bacteria to better exploit surface area contributed by texturing, overriding the geometric constraints and antibiofouling effects of sub-bacterial feature size and spacing (Friedlander, et al., 2013). This is further enhanced by the flagella’s motility function, which helps bacteria to seek out improved surface access (Friedlander, et al., 2013; Hou, et al., 2011). It thus seems that the physical mechanism by which these fracture surfaces operate is limited to less complex bacteria that lack extracellular appendages. This is true of *S. aureus*, tested in this study, which is non-flagellated and non-motile (Valle, et al., 2015). Other, more complex bacteria such as *E. coli* may not be as susceptible to antibiofouling by the simple, physical mechanism of the fracture surfaces. Another limitation of the findings is regarding the duration of the study. To assess whether or not these fracture textures are able to disrupt biofilm formation sufficiently, a long-term study ( $\sim 21$  days) would be required as exemplified by Chung, et al. (2007). This is beyond the scope of the present research, which focuses on attachment-stage antibiofouling.

Most notably, the present study has discovered a novel avenue to elicit topography-mediated antibiofouling property. We have demonstrated the antibiofouling property of a fracture surface, which can be enhanced or suppressed by adjusting cross-head speed. Importantly, this occurs without chemical modification, and is hence primarily by the action of physical mechanisms related to topography. The findings fall in line with earlier work and

can be explained by consideration of cell-surface interfacial area and the attachment point theory.

#### 4. CONCLUSIONS

In this work, a Ti-6Al-4V textured surface was manufactured by tensile fracture at different cross-head speeds, ranging from quasi-static to dynamic. The fracture surfaces were characterised and subsequently treated with *S. aureus* to assess bacterial attachment. Fractographic study of the surface indicated the presence of dual-mode fracture, underpinned by the alloy's  $\alpha$  and  $\beta$  phases, thus producing regions of ductile, microvoid coalescence and brittle, cleavage facets. Based on load-extension curves, quantitative roughness data, and qualitative SEM visualisation, it was evident that cross-head speed modulated the dual-mode fracture such that increased speed exacerbated brittle fracture and cleavage faceting, whilst slower speeds produced ductile fracture and microvoid coalescence. In line with the attachment point theory, highly textured microvoids possessed appreciable antibiofouling property, whilst featureless cleavage facets did not. Accordingly, fracture at high cross-head speeds (100mm/min), with high proportion of cleavage, resulted in no significant antibiofouling. Only fracture at lower cross-head speeds (1mm/min and 10mm/min), which were microvoid-dominant, yielded significant reduction in attachment. The greatest reduction (~72%) was achieved at a cross-head speed of 1mm/min. Ultimately, this research has brought to light a novel, yet simple, technique for topography-mediated antibiofouling property, contributing knowledge toward the pursuit of innovative antibacterial surfaces for biomedical application.

#### ACKNOWLEDGEMENTS

The authors would like to acknowledge the following QUT personnel: Ph.D. candidate, Ms. Alka Jaggessar, for her kind assistance with bacterial assays; and senior technician and materials specialist, Mr. Gregory Paterson, for his help with INSTRON testing equipment. This research was supported by equipment, facilities and services at QUT's Central Analytical Research Facility (CARF), Institute of Health and Biomedical Innovation (IHBI), and Design and Manufacturing Centre (DMC).

**AUTHOR CONTRIBUTION**

All authors made noteworthy contribution to the article. The study was originally conceptualised by P.Y. and P.H. and was further refined and designed into a methodology by A.V. Manufacture, characterisation and bacterial study was carried out by A.V., with the assistance of P.H., who provided valuable technical expertise with electron microscopy and image analysis, and also A.M., who helped design and execute the bacterial study methodology. A.V. analysed and interpreted the results to derive the conclusions. The manuscript and figures were formatted and prepared by A.V. All authors carried out review and editing. Ongoing support and supervision was facilitated by P.Y.

**DECLARATION OF INTEREST**

None: the authors have no competing interests to declare regarding the authorship, funding and publication of this article.

**FUNDING SOURCES**

This work was funded by the Queensland University of Technology (QUT) Research Training Program (RTP) stipend.

**REFERENCES**

- ASTM International. (2015). *B265-15 Standard Specification for Titanium and Titanium Alloy Strip, Sheet, and Plate*. West Conshohocken, PA.
- ASTM International. (2016). *E8/E8M-16a Standard Test Methods for Tension Testing of Metallic Materials*. West Conshohocken, PA.
- Attar, H., Calin, M., Zhang, L. C., Scudino, S., & Eckert, J. (2014). Manufacture by selective laser melting and mechanical behavior of commercially pure titanium. *Materials Science and Engineering: A*, 593(Supplement C), 170-177. doi: <https://doi.org/10.1016/j.msea.2013.11.038>

- Barthlott, W., & Neinhuis, C. (1997). Purity of the sacred lotus, or escape from contamination in biological surfaces. *Planta*, 202(1), 1-8. doi: 10.1007/s004250050096
- Bixler, G. D., Theiss, A., Bhushan, B., & Lee, S. C. (2014). Anti-fouling properties of microstructured surfaces bio-inspired by rice leaves and butterfly wings. *Journal of Colloid and Interface Science*, 419, 114-133. doi: <https://doi.org/10.1016/j.jcis.2013.12.019>
- Boyce, J. M. (2007). Environmental contamination makes an important contribution to hospital infection. *Journal of Hospital Infection*, 65(Supplement 2), 50-54. doi: [https://doi.org/10.1016/S0195-6701\(07\)60015-2](https://doi.org/10.1016/S0195-6701(07)60015-2)
- Boyle, K. E., Heilmann, S., van Ditmarsch, D., & Xavier, J. B. (2013). Exploiting social evolution in biofilms. *Current Opinion in Microbiology*, 16(2), 207-212. doi: <https://doi.org/10.1016/j.mib.2013.01.003>
- Brown, E. D., & Wright, G. D. (2016). Antibacterial drug discovery in the resistance era. *Nature*, 529(7586), 336-343. doi: 10.1038/nature17042
- Callow, M. E., Jennings, A. R., Brennan, A. B., Seegert, C. E., Gibson, A., Wilson, L., . . . Callow, J. A. (2002). Microtopographic Cues for Settlement of Zoospores of the Green Fouling Alga *Enteromorpha*. *Biofouling*, 18(3), 229-236. doi: 10.1080/08927010290014908
- Campbell, F. C. (2012). *Fatigue and fracture understanding the basics*. Materials Park, Ohio: ASM International.
- Carman, M. L., Estes, T. G., Feinberg, A. W., Schumacher, J. F., Wilkerson, W., Wilson, L. H., . . . Brennan, A. B. (2006). Engineered antifouling microtopographies – correlating wettability with cell attachment. *Biofouling*, 22(1), 11-21. doi: 10.1080/08927010500484854
- Chung, K. K., Schumacher, J. F., Sampson, E. M., Burne, R. A., Antonelli, P. J., & Brennan, A. B. (2007). Impact of engineered surface microtopography on biofilm formation of *Staphylococcus aureus*. *Biointerphases*, 2(2), 89-94. doi: 10.1116/1.2751405

- Davies, J., & Davies, D. (2010). Origins and evolution of antibiotic resistance. *Microbiol Mol Biol Rev*, 74(3), 417-433. doi: 10.1128/MMBR.00016-10
- Dunne, W. M. (2002). Bacterial Adhesion: Seen Any Good Biofilms Lately? *Clinical Microbiology Reviews*, 15(2), 155-166. doi: 10.1128/CMR.15.2.155-166.2002
- Elias, C. N., Lima, J. H. C., Valiev, R., & Meyers, M. A. (2008). Biomedical applications of titanium and its alloys. *JOM*, 60(3), 46-49. doi: 10.1007/s11837-008-0031-1
- Everaerts, J., Verlinden, B., & Wevers, M. (2016). The influence of the alpha grain size on internal fatigue crack initiation in drawn Ti-6Al-4V wires. *Procedia Structural Integrity*, 2, 1055-1062. doi: <https://doi.org/10.1016/j.prostr.2016.06.135>
- Fadeeva, E., Truong, V. K., Stiesch, M., Chichkov, B. N., Crawford, R. J., Wang, J., & Ivanova, E. P. (2011). Bacterial retention on superhydrophobic titanium surfaces fabricated by femtosecond laser ablation. *Langmuir*, 27(6), 3012-3019. doi: 10.1021/la104607g
- Fiorucci, M. P., López, A. J., & Ramil, A. (2015). Surface modification of Ti6Al4V by nanosecond laser ablation for biomedical applications. *Journal of Physics: Conference Series*, 605(1), 012022. Retrieved from <http://stacks.iop.org/1742-6596/605/i=1/a=012022>
- Follansbee, P. S., & Gray, G. T. (1989). An analysis of the low temperature, low and high strain-rate deformation of Ti-6Al-4V. *Metallurgical Transactions A*, 20(5), 863-874. doi: 10.1007/BF02651653
- Friedlander, R. S., Vlamakis, H., Kim, P., Khan, M., Kolter, R., & Aizenberg, J. (2013). Bacterial flagella explore microscale hummocks and hollows to increase adhesion. *Proceedings of the National Academy of Sciences*, 110(14), 5624-5629. doi: 10.1073/pnas.1219662110
- Gerberich, W., & Yang, W. (2003). Interfacial and Nanoscale Failure In I. Milne, R. O. Ritchie & B. Karihaloo (Eds.), *Comprehensive Structural Integrity* (Vol. 8, pp. 1-40). Oxford: Pergamon.

- Hasan, J., Crawford, R. J., & Ivanova, E. P. (2013). Antibacterial surfaces: the quest for a new generation of biomaterials. *Trends in Biotechnology*, *31*(5), 295-304. doi: <http://dx.doi.org/10.1016/j.tibtech.2013.01.017>
- Hoipkemeier-Wilson, L., Schumacher, J. F., Carman, M. L., Gibson, A. L., Feinberg, A. W., Callow, M. E., . . . Brennan, A. B. (2004). Antifouling Potential of Lubricious, Micro-engineered, PDMS Elastomers against Zoospores of the Green Fouling Alga *Ulva* (Enteromorpha). *Biofouling*, *20*(1), 53-63. doi: 10.1080/08927010410001662689
- Hou, S., Gu, H., Smith, C., & Ren, D. (2011). Microtopographic Patterns Affect *Escherichia coli* Biofilm Formation on Poly(dimethylsiloxane) Surfaces. *Langmuir*, *27*(6), 2686-2691. doi: 10.1021/la1046194
- Ivanova, S. G., Biederman, R. R., & Sisson, R. D. (2002). Investigation of fatigue crack initiation in Ti-6Al-4V during tensile-tensile fatigue. *Journal of Materials Engineering and Performance*, *11*(2), 226-231. doi: 10.1361/105994902770344312
- Katsikogianni, M. (2004). Concise review of mechanisms of bacterial adhesion to biomaterials and of techniques used in estimating bacteria-material interactions. *European cells & materials*, *8*(3), 37. Retrieved from
- Klein, E., Smith, D. L., & Laxminarayan, R. (2007). Hospitalizations and Deaths Caused by Methicillin-Resistant *Staphylococcus aureus*, United States, 1999–2005. *Emerging Infectious Disease journal*, *13*(12), 1840. doi: 10.3201/eid1312.070629
- Komaromy, A. Z., Li, S., Zhang, H., Nicolau, D. V., Boysen, R. I., & Hearn, M. T. W. (2012). Arrays of nano-structured surfaces to probe the adhesion and viability of bacteria. *Microelectronic Engineering*, *91*, 39-43. doi: <https://doi.org/10.1016/j.mee.2011.10.012>
- Kumar, A., Roberts, S., & Wilkinson, A. (2007). *Low-temperature fracture mechanisms in a spheroidised reactor pressure vessel steel* (Vol. 144).
- Lafuma, A., & Quere, D. (2003). Superhydrophobic states. [10.1038/nmat924]. *Nat Mater*, *2*(7), 457-460. Retrieved from <http://dx.doi.org/10.1038/nmat924>

- Lee, W. S., Chen, T. H., Lin, C. F., & Lu, G. T. (2010). Adiabatic Shearing Localisation in High Strain Rate Deformation of Al-Sc Alloy. *MATERIALS TRANSACTIONS*, 51(7), 1216-1221. doi: 10.2320/matertrans.M2010053
- Lee, W. S., Lin, C. F., & Huang, S. Z. (2006). Effect of temperature and strain rate on the shear properties of Ti-6Al-4V alloy. *Proceedings of the Institution of Mechanical Engineers, Part C: Journal of Mechanical Engineering Science*, 220(2), 127-136. doi: 10.1243/09544062C05505
- Lora-Tamayo, J., Murillo, O., Iribarren, J. A., Soriano, A., Sánchez-Somolinos, M., Baraia-Etxaburu, J. M., . . . Pérez, F. (2013). A Large Multicenter Study of Methicillin-Susceptible and Methicillin-Resistant Staphylococcus aureus Prosthetic Joint Infections Managed With Implant Retention. *Clinical Infectious Diseases*, 56(2), 182-194. doi: 10.1093/cid/cis746
- Montanaro, L., Speziale, P., Campoccia, D., Ravaioli, S., Cangini, I., Pietrocola, G., . . . Arciola, C. R. (2011). Scenery of Staphylococcus implant infections in orthopedics. *Future Microbiology*, 6(11), 1329-1349. doi: 10.2217/fmb.11.117
- Mudry, F. (1987). A local approach to cleavage fracture. *Nuclear Engineering and Design*, 105(1), 65-76. doi: [https://doi.org/10.1016/0029-5493\(87\)90230-5](https://doi.org/10.1016/0029-5493(87)90230-5)
- Murr, L. E., Quinones, S. A., Gaytan, S. M., Lopez, M. I., Rodela, A., Martinez, E. Y., . . . Wicker, R. B. (2009). Microstructure and mechanical behavior of Ti-6Al-4V produced by rapid-layer manufacturing, for biomedical applications. *Journal of the Mechanical Behavior of Biomedical Materials*, 2(1), 20-32. doi: <https://doi.org/10.1016/j.jmbbm.2008.05.004>
- Neely, A. N., & Maley, M. P. (2000). Survival of Enterococci and Staphylococci on Hospital Fabrics and Plastic. *Journal of Clinical Microbiology*, 38(2), 724-726. Retrieved from <http://www.ncbi.nlm.nih.gov/pmc/articles/PMC86187/>
- Parrington, R. J. (2002). Fractography of metals and plastics. *Practical Failure Analysis*, 2(5), 16-19. doi: 10.1007/BF02715463
- Patil, S., Kekade, S., Phapale, K., Jadhav, S., Powar, A., Supare, A., & Singh, R. (2016). Effect of  $\alpha$  and  $\beta$  Phase Volume Fraction on Machining Characteristics of Titanium

Alloy Ti6Al4V. *Procedia Manufacturing*, 6, 63-70. doi: <https://doi.org/10.1016/j.promfg.2016.11.009>

Petronis, Š., Berntsson, K., Gold, J., & Gatenholm, P. (2000). Design and microstructuring of PDMS surfaces for improved marine biofouling resistance. *Journal of Biomaterials Science, Polymer Edition*, 11(10), 1051-1072. doi: 10.1163/156856200743571

Piveta, A. C. G., Montandon, A. A. B., Ricci, W. A., & Nagle, M. M. (2012). Mechanical strength and analysis of fracture of titanium joining submitted to laser and tig welding. *Materials Research*, 15, 937-943. Retrieved from [http://www.scielo.br/scielo.php?script=sci\\_arttext&pid=S1516-14392012000600016&nrm=iso](http://www.scielo.br/scielo.php?script=sci_arttext&pid=S1516-14392012000600016&nrm=iso)

Pokluda, J., & Šandera, P. (2010). *Micromechanisms of Fracture and Fatigue*: Springer, London.

Rack, H. J., & Qazi, J. I. (2006). Titanium alloys for biomedical applications. *Materials Science and Engineering: C*, 26(8), 1269-1277. doi: <https://doi.org/10.1016/j.msec.2005.08.032>

Ribeiro, M., Monteiro, F. J., & Ferraz, M. P. (2012). Infection of orthopedic implants with emphasis on bacterial adhesion process and techniques used in studying bacterial-material interactions. *Biomatter*, 2(4), 176-194. doi: 10.4161/biom.22905

Scardino, A. J., & de Nys, R. (2011). Mini review: Biomimetic models and bioinspired surfaces for fouling control. *Biofouling*, 27(1), 73-86. doi: 10.1080/08927014.2010.536837

Scardino, A. J., Guenther, J., & de Nys, R. (2008). Attachment point theory revisited: the fouling response to a microtextured matrix. *Biofouling*, 24(1), 45-53. doi: 10.1080/08927010701784391

Scardino, A. J., Harvey, E., & De Nys, R. (2006). Testing attachment point theory: diatom attachment on microtextured polyimide biomimics. *Biofouling*, 22(1-2), 55-60. doi: 10.1080/08927010500506094

- Schumacher, J. F., Carman, M. L., Estes, T. G., Feinberg, A. W., Wilson, L. H., Callow, M. E., . . . Brennan, A. B. (2007). Engineered antifouling microtopographies - effect of feature size, geometry, and roughness on settlement of zoospores of the green alga *Ulva*. *Biofouling*, *23*(1-2), 55-62. doi: 10.1080/08927010601136957
- Truong, V. K., Webb, H. K., Fadeeva, E., Chichkov, B. N., Wu, A. H. F., Lamb, R., . . . Ivanova, E. P. (2012). Air-directed attachment of coccoid bacteria to the surface of superhydrophobic lotus-like titanium. *Biofouling*, *28*(6), 539-550. doi: 10.1080/08927014.2012.694426
- Valle, J., Burgui, S., Langheinrich, D., Gil, C., Solano, C., Toledo-Arana, A., . . . Lasa, I. (2015). Evaluation of Surface Microtopography Engineered by Direct Laser Interference for Bacterial Anti-Biofouling. *Macromolecular Bioscience*, *15*(8), 1060-1069. doi: 10.1002/mabi.201500107
- Vasudevan, R., Kennedy, A. J., Merritt, M., Crocker, F. H., & Baney, R. H. (2014). Microscale patterned surfaces reduce bacterial fouling-microscopic and theoretical analysis. *Colloids and Surfaces B: Biointerfaces*, *117*, 225-232. doi: <https://doi.org/10.1016/j.colsurfb.2014.02.037>
- Vega, N. M., & Gore, J. (2014). Collective antibiotic resistance: mechanisms and implications. *Current Opinion in Microbiology*, *21*, 28-34. doi: <https://doi.org/10.1016/j.mib.2014.09.003>
- Vickery, K., Deva, A., Jacombs, A., Allan, J., Valente, P., & Gosbell, I. B. (2012). Presence of biofilm containing viable multiresistant organisms despite terminal cleaning on clinical surfaces in an intensive care unit. *Journal of Hospital Infection*, *80*(1), 52-55. doi: <https://doi.org/10.1016/j.jhin.2011.07.007>
- Weber, D. J., Rutala, W. A., Miller, M. B., Huslage, K., & Sickbert-Bennett, E. (2010). Role of hospital surfaces in the transmission of emerging health care-associated pathogens: Norovirus, *Clostridium difficile*, and *Acinetobacter* species. *American Journal of Infection Control*, *38*(5, Supplement), S25-S33. doi: <https://doi.org/10.1016/j.ajic.2010.04.196>
- Weinstein, R. A., & Hota, B. (2004). Contamination, Disinfection, and Cross-Colonization: Are Hospital Surfaces Reservoirs for Nosocomial Infection? *Clinical Infectious Diseases*, *39*(8), 1182-1189. doi: 10.1086/424667

- Whitehead, K. A., Colligon, J., & Verran, J. (2005). Retention of microbial cells in substratum surface features of micrometer and sub-micrometer dimensions. *Colloids and Surfaces B: Biointerfaces*, 41(2), 129-138. doi: <https://doi.org/10.1016/j.colsurfb.2004.11.010>
- Xu, L.-C., & Siedlecki, C. A. (2012). Submicron-textured biomaterial surface reduces staphylococcal bacterial adhesion and biofilm formation. *Acta Biomaterialia*, 8(1), 72-81. doi: <https://doi.org/10.1016/j.actbio.2011.08.009>
- Yang, L., Wang, B.-y., Lin, J.-g., Zhao, H.-j., & Ma, W.-y. (2015). Ductile fracture behavior of TA15 titanium alloy at elevated temperatures. *International Journal of Minerals, Metallurgy, and Materials*, 22(10), 1082-1091. doi: 10.1007/s12613-015-1171-2
- Zhang, B., Luo, Y., Pearlstein, A. J., Aplin, J., Liu, Y., Baughan, G. R., . . . Millner, P. D. (2014). Fabrication of Biomimetically Patterned Surfaces and Their Application to Probing Plant–Bacteria Interactions. *ACS Applied Materials & Interfaces*, 6(15), 12467-12478. doi: 10.1021/am502384q

#### HIGHLIGHTS:

- A Ti-6Al-4V textured surface was manufactured by tensile fracture at three different cross-head speeds (1mm/min, 10mm/min and 100mm/min).
- Higher fracture speeds produced a higher proportion of brittle, cleavage facets, whilst lower fracture speeds produced a higher proportion of ductile, microvoid coalescence.
- Regions of coalesced microvoids possessed inherent, topography-mediated antibiofouling property, as described by the attachment point theory.
- Statistically significant reduction of *Staphylococcus aureus* attachment was achieved with cross-head speeds of 1mm/min (72%) and 10mm/min (43%), relative to an unmodified control surface.
- Antibiofouling property can be elicited simply by fracture, and controlled (enhanced or suppressed) further by fracture speed.